A mild Neurofibromatosis type 1 phenotype produced by the combination of the benign nature of a leaky *NF1*-splice mutation and the presence of a complex mosaicism

Juana Fernández-Rodríguez[1,*], Joan Castellsagué[1,*], Llúcia Benito[2], Yolanda Benavente[3,4], Gabriel Capellà[1], Ignacio Blanco[2], Eduard Serra[5] and Conxi Lázaro[1]

* These two authors contributed equally to the study

[1]Hereditary Cancer Program, Genetic Diagnosis Unit; [2]Hereditary Cancer Program, Genetic Counseling Unit; [3]Unit of Infections and Cancer (UNIC), Cancer Epidemiology Research Program; all three at Institut Català d'Oncologia (ICO-IDIBELL); [4]CIBER de Epidemiología y Salud Pública (CIBERESP), Spain; [5]L'Institut de Medicina Predictiva i Personalitzada del Càncer (IMPPC), Badalona, Barcelona, Spain.

*Correspondence to Conxi Lázaro, Ph.D., Hereditary Cancer Program, Genetic Diagnosis Unit, Laboratori de Recerca Translacional, Institut Català d'Oncologia-ICO-IDIBELL, Hospital Duran i Reynals, Gran Via 199-203, L'Hospitalet de Llobregat, 08907, Spain. Tel.: +34932607342; Fax: +34932607466; E-mail: clazaro@iconcologia.net

ABSTRACT

Here we analyze the genetic and molecular basis responsible for a very benign phenotype observed in a NF1 patient. Quantification of cells carrying the *NF1* mutation in different samples derived from the three embryonic layers revealed mosaicism. Furthermore, the construction of a minigene with patient's mutation (c.3198-314G>A) confirmed its benign nature due to the leakiness of the splicing mechanism that generated a proportion of correctly spliced transcripts. Hence, we concluded that the mild phenotype observed in this patient is the result of the presence of mosaicism together with the benign nature of a leaky *NF1*-splice mutation. Finally, with the aim of developing a personalized therapeutic approach for this patient, we demonstrated correction of the splicing defect by using specific antisense morpholino oligomers. Our results provide an example of the molecular complexity behind disease phenotypes and highlight the importance of using comprehensive genetic approaches to better assess phenotype-genotype correlations.

Neurofibromatosis type 1 (NF1; MIM#162200) is an autosomal dominant disorder characterized by an increased predisposition to develop certain types of malignancies as well as by the presence of a wide range of clinical traits involving cells of neural crest origin (reviewed in Riccardi, 1992). NF1 is caused by germline mutations in the *NF1* gene, which is one of the human genes with a higher mutation rate. Comprehensive genetic studies identified more than 1,100 disease-causing mutations allowing a precise depiction of the *NF1* germline mutational spectrum (reviewed in Messiaen, 2008). So far, two constitutive *NF1* mutations have been correlated with a particular NF1 phenotype. Individuals with type 1 *NF1*-deletions, which encompass 1.4 Mb of genomic DNA [Kayes, et al., 1994; Lopez Correa, et al., 1999] and involve several other genes in addition to the *NF1*, are characterized by a severe phenotype, consisting of learning problems, dysmorphic features and a high number of dermal neurofibromas [Mautner, et al., 2010; Pasmant, et al., 2010]. By contrast, patients with the recurrent c.2970-2972 delAAT mutation seem to express a moderate phenotype characterized by the absence of dermal neurofibromas [Upadhyaya, et al., 2007].

It has been suggested that a proportion of the new mutations are actually somatic implying than some sporadic patients are mosaics for a *NF1* mutation [Kehrer-Sawatzki and Cooper, 2008; Zlotogora, 1993]. Depending on the stage during development of the occurrence of the mutation we can distinguish patients showing generalized mosaicism, segmental mosaicism and gonadal mosaicism [Ruggieri and Huson, 2001]. Generalized mosaicism cases exhibit typical symptoms of the disease in a mild generalized form, making them very difficult to distinguish from non-mosaic patients. Segmental manifestation show clinical manifestations limited to one or a few areas of the body [Crowe, et al., 1956; Moss and Green, 1994; Riccardi, 1982], this is a rare condition which occurs at around 1:36,000-40,000 individuals [Friedman JM, et al., 1999 ; Ingordo, et al., 1995; Ruggieri and Polizzi, 2000; Wolkenstein, et al., 1995]. Gonadal mosaicism is confined to the germline and is extremely uncommon in NF1 [Bottillo, et al., 2010; Lazaro, et al., 1994]. Identification of somatic mosaicism and

assessment of tissues affected by the *NF1* somatic mutation is difficult and represents a challenge because it is especially important for providing accurate genetic counselling to the patient.

For several genetic conditions, genotype-phenotype studies have suggested the importance of mechanisms regulating splicing as modifiers of phenotype in carriers of splicing defects [Nissim-Rafinia and Kerem, 2005]. For instance, a leaky effect of some splicing mutations associated with the production of wild-type transcripts from mutated alleles has been described. In some cases this phenomenon has been associated with a mild phenotype [Beck, et al., 1999]. The high number and diversity of splicing mutations in the *NF1* gene made it interesting to explore the occurrence of leakiness in the splicing mechanism and its putative relation to the severity of the disease.

In this work we describe the molecular basis underlying the mild NF1 phenotype of a patient fulfilling the NIH-NF1 established diagnostic criteria. Written informed consent was obtained from the patient following our institutional review board approved protocol. The patient is a 34-year-old woman who is a sporadic case of the disease (Figure 1A, left panel) showing 20 café-au-lait spots on the trunk and upper extremities, mild scoliosis, axillary and submammary freckling, and presence of less than 50 minuscule neurofibromas (a few millimeters in diameter) located on the trunk, which started to appear when she was 18 years old (Figure 1A, right panel). The patient does not have Lisch nodules, any dysmorphism or learning disability. The *NF1*-mutational analysis using DNA isolated from peripheral blood of the patient revealed a point mutation in intron 19a of the gene (c.3198-314G>A) (Supp. Table S1). This mutation is a deep intronic mutation that creates a new cryptic acceptor splice site that uses two different cryptic donor splice sites present in the wild-type sequence (Supp. Table S2), to generate two aberrantly spliced transcripts showing inclusion of two different cryptic exons (Figure 1B); both cryptic exons would generate the same putative truncated protein (p.Asp1067TrpfsX7).

We investigated two possible biological mechanisms that could explain the mild phenotype of the patient: somatic mosaicism and presence of mild *NF1*-mutation. To explore mosaicism we used a quantitative approach, based on the analysis of a single nucleotide primer extension reaction (SNaPShot analysis), to determine the proportion of cells containing the mutated allele in a subset of samples representative of the three embryonic layers. As this *NF1* mutation had never been described before in other patients, it was impossible to obtain genetic material representative of a bona fide heterozygous sample that could be used as a control for quantification. Hence, we generated artificial controls consisting of two plasmids; one containing the patient's mutation and the other bearing the wild type sequence. A mixture of serial proportions of both plasmids was used to obtain a standard curve that allowed estimation of the proportion of mutant alleles present in the different tissues obtained from the patient (Supp. Figures S1 and S2). This analysis revealed that samples derived from the endoderm and mesoderm, such as uroepithelial cells and peripheral blood respectively, showed a proportion of mutant allele of around 50% (Figure 1C and Supp. Figure S3), indicating that all the cells from these tissues are carrying the mutation in heterozygosis. However, samples derived from the ectoderm, such as skin, buccal swab or hair roots, showed a mutant allele proportion lower than 50%, ranging from 20% to 35%, suggesting that only a proportion of the cells of these tissues were carrying the *NF1* mutation. Cells from saliva showed an intermediate value that was in agreement with its nature, consisting of a mixture of white blood cells (mesoderm) plus buccal epithelial cells (ectoderm). To validate our results and confirm that the observed different proportions of mutated and WT alleles in the SNaPShot analysis were reflecting a somatic mosaicism and were not caused by amplification artefacts due to the different nature and origin of DNAs analyzed, we performed a control SNaPShot analysis using a SNP unrelated to the disease in the same set of DNA samples. We studied SNP rs2075786 located in an intronic region of the *hTERT* gene, located on a different human chromosome and for which our patient was heterozygous. In this case,

the proportion of both alleles was close to 50% in all tested DNA samples (Figure 1C and Supp. Figure S4), a result that reinforced the validity of our previous results observed in the SNaPShot analysis of the *NF1* mutation. Taking all our results together we can conclude that the patient studied here is a case of a NF1 mosaicism as the *NF1* mutation is present in different proportions in different cell types. Hence, this *NF1* mutation may have occurred early during development; as cells derived from the three embryonic layers are carrying the mutation in contrast to cases of segmental mosaicism, where the proportion of mutated cells in non-neural crest derived tissues can often lie below the detection level of routine analysis [Maertens, et al., 2007]. Although several cases of mosaicism have been described for NF1, the role of mosaicism in NF1 is still scarcely analyzed and limited to few number of cases [Kehrer-Sawatzki and Cooper, 2008]. The use of different methodological approaches with high sensitivity such as SNaPShot analysis or real time quantitative allele discrimination [Aretz, et al., 2007; Maertens, et al., 2006], together with the investigation of several different tissues in cases where a mild form of the disease is observed, will help to ascertain the role of somatic mosaicism in Neurofibromatosis type 1.

Taking into consideration the embryological origin of the different tissues analyzed and the fact that the majority of NF1 traits have a neural crest-derived cell origin (reviewed in Raedt et al., 2008), we were surprised by the proportions of mutated cells identified, greater in tissues mainly derived from the endoderm or mesoderm and smaller in tissues derived form the ectoderm. We decided to further explore the complex mosaicism exhibited in this patient by performing an X-chromosome inactivation (XCI) assay in the same set of tissues [Allen, et al., 1992]. X-chromosome inactivation is a stochastic event that occurs in the early stages of embryonic development in female embryos [Lyon, 1961; Lyon, 1962]. If a genetic mutation occurs after this inactivation, one can perform an X-chromosome inactivation test in different tissues in order to ascertain whether any bias is observed in the proportion of inactivation in both X-chromosomes and compare these results to the proportion of

cells carrying the given genetic mutation [Wang, et al., 2009]. In our case, determination of clonal expansion was based on the analysis of DNA methylation and CAG tandem repeats at the human androgen receptor locus (*HUMARA*) [Allen, et al., 1992], located on chromosome X, in the same tissues were mutation analysis was performed (with the exceptions of skin and hair roots). The number of CAG repeats differentiated the parental X chromosomes and methylation status distinguished the active and inactive X chromosome. In the absence of proliferative differences (advantages or disadvantages) between *NF1*-mutated and non-mutated cells, completely random XCI would be expected to result in around 50% inactivation of each X chromosome in all tissues. By convention, mildly skewed XCI was defined by an allele ratio 80-90% skewed inactivation, and extremely skewed XCI was defined by an allele ratio >90% skewed inactivation [Beever, et al., 2003; Kimani, et al., 2007]. Interestingly, we observed skewed XCI in the case of peripheral blood, saliva and uroepithelial cells with ratios of 12:88; 15:85 and 10:90, respectively. None of the rest of tissues from the patient, or a subset of control blood DNA samples, showed skewed XCI (Figure 1D and Supp. Figure S5). Tissues carrying the highest proportion of mutated cells coincided with those exhibiting skewed XCI. Moreover, in all these tissues, the same X chromosome was predominantly inactivated, making it unlikely that this observed skewed X- inactivation was the result of a purely random process. These results suggest a proliferative advantage of certain cells carrying the *NF1* mutation that results in higher proportions of both percentage of mutated cells and cells with skewed X chromosome inactivation. Consequently, these proliferative differences suggest that the observed proportions of mutated cells in the adult tissues analyzed in the present study do not reflect the initial percentage of mutated cells in the different embryonic cell layers. However these results have to be taken carefully as it has been reported that X-inactivation ratios may vary between different tissues within one normal individual [Sharp, et al., 2000].

To investigate a second possible cause of the observed mild NF1 phenotype, the benign nature of the constitutional *NF1* mutation, we analyzed and quantified the expression of mutant transcripts produced by the deep intronic *NF1* mutation identified, exploring different tissues from the same patient. We analyzed any deviation from the expected 50:50 proportion of mutant *versus* normal transcripts, taking into consideration the proportion of mutated cells identified in the analysis of DNA from different tissues. The analysis of RNA from fresh tissues indicated, with a certain degree of variation between samples, a low proportion of mutated transcripts, ranging from 1.4% to 14.41% and none in the hair root sample (Figure 2A upper panel). The study of cell cultures (lymphocytes and fibroblasts) revealed a low proportion of mutated transcripts as well as the action of the nonsense-mediated mRNA decay (NMD) mechanism on mutated-mRNA, since puromycin treatment was able to increase the levels of mutant transcripts observed in both cell types (Figure 2A bottom panel). By comparing the proportion of mutated transcripts (Figure 2A) with the percentage of mutated DNA (Figure 1C) in the same tissues, it became clear that there was a reduction in the proportion of mutated RNA. An illustrative example was the analysis of lymphocyte cells that showed equal proportions of mutated and wild-type alleles at the DNA level. However the analysis of their transcriptional profile provides evidence of a much lower proportion of aberrantly spliced transcripts than the expected 50% (20% after puromycin treatment and less than 10% without this treatment). Altogether, the differences between observed and expected proportions of aberrantly spliced transcripts, even after avoiding NMD, suggested the possibility that wild-type transcripts were also produced from the mutated allele, resulting in a low proportion of abnormal transcripts. In order to confirm this hypothesis we also constructed a minigene carrying the mutated allele. The analysis of the transcripts generated by the minigene containing mutation c.3198-314G>A indicated the production of both mutated and wild-type transcripts, while the minigene encoding the normal sequence only produced normal transcripts (Figure 2B and Supp. Figure S6), confirming that the low

proportion of mutant transcripts is due to the production of normal transcripts from the mutated allele due to leakiness of the splicing mechanism. Therefore, the particular benign nature of this *NF1* mutation was possibly contributing to the mild phenotype observed in our patient, by acting as a hypomorphic allele rather than a null one.

Finally, and with the aim of starting to design personalized therapeutic strategies for NF1 patients, three different specific AMOs blocking cryptic splice sites used by the mutation were designed (as previously reported) [Pros, et al., 2009]. AMOs were designed, synthesized, and purified by Gene Tools (Philomath, OR) and endo-porter (GeneTools) was used to deliver AMOs into skin-derived fibroblasts from the patient. We observed that the three designed AMOs were able to reduce the levels of mutant transcripts although a complete correction was only observed when a combination of the three AMOs was used (Figure 2C upper panel) as has also been described in other genetic disorders [Gurvich, et al., 2008]. To confirm that this reduction was specific to the AMO designed we performed the same treatment but using an unspecific AMO, designed to block a donor splice site generated by a different mutation located in intron 3 of the *NF1* gene. As expected, no effect on the proportion of mutant transcripts was observed when using an unspecific AMO. Furthermore, we observed that IVS19a-AMO donors 1 and 2 inhibit, in a specific manner, the two aberrant transcripts generated. IVS19a-AMO donor 1 preferentially inhibits aberrant transcript 1 (r.3197-3198ins3198-214-3198-312) whereas IVS19a-AMO donor 2 preferentially inhibits aberrant transcript 2 (r.3197-3198ins3198-245-3198-312) (Supp. Figure S7). Finally, to confirm that correction of aberrant splicing by AMO treatment at RNA level had some effect at a functional level, we indirectly assessed neurofibromin function, by measuring levels of active Ras (Ras-GTP) as an indicator of neurofibromin GTPase activity. We treated primary fibroblast cultures carrying the deep intronic mutation firstly with one AMO blocking the newly created acceptor splice site and secondly with a combination of three AMOs that were designed to block all cryptic splice sites located at intron 19a. We found that levels of Ras-GTP were lower in

fibroblasts treated with specific AMOs than in untreated fibroblast or in fibroblasts treated with an unspecific AMO (Figure 2C lower panel), in agreement with our previous results using cell lines derived from other NF1 patients carrying the same type of mutation [Pros, et al., 2009]. This decrease in active Ras levels suggests that AMO treatment was indeed restoring neurofibromin GTPase function.

To conclude, in this report we are presenting a very illustrative case where a combination of different biological processes such as somatic mosaicism and the leaky nature of a splicing mutation, are the possible causes of the mild NF1 phenotype observed in our patient. Our results highlight the complexity of genotype-phenotype correlations and the importance of performing comprehensive genetic studies to interpret clinical findings and facilitate genetic counselling.

ACKNOWLEDGEMENTS

We thank the patient described in this study for her willingness to participate and collaborate in all the proposed experiments. We thank Dr. Laura Valle and Núria Seguí for providing us conditions and reagents to analyse the telomerase SNP. We thank Susan Huson and Harvey Evans for critical advice and corrections of the manuscript. Authors would like to especially acknowledge the *Asociación Española de Afectados de Neurofibromatosis*, who awarded us one of their grants, as well as giving their constant support for our research. We would like also to thank the *Asociación Española contra el Cáncer* that recognize our group as a one of the *Grupos Estables de Investigación Oncológica 2010*. Contract grant sponsor: Spanish Health Research Fund; Carlos III Health Institute; Catalan Health Institute and Autonomous Government of Catalonia. Contract grant numbers: ISCIIIRETIC: RD06/0020/1051, RD06/0020/1050, 2009SGR290, PI10/01422, CA08/00248.

References

Allen RC, Zoghbi HY, Moseley AB, Rosenblatt HM, Belmont JW. 1992. Methylation of HpaII and HhaI sites near the polymorphic CAG repeat in the human androgen-receptor gene correlates with X chromosome inactivation. Am J Hum Genet 51(6):1229-39.

Aretz S, Stienen D, Friedrichs N, Stemmler S, Uhlhaas S, Rahner N, Propping P, Friedl W. 2007. Somatic APC mosaicism: a frequent cause of familial adenomatous polyposis (FAP). Hum Mutat 28(10):985-92.

Beck S, Penque D, Garcia S, Gomes A, Farinha C, Mata L, Gulbenkian S, Gil-Ferreira K, Duarte A, Pacheco P, Barreto C, Lopes B, Cavaco J, Lavinha J, Amaral MD. 1999. Cystic fibrosis patients with the 3272-26A-->G mutation have mild disease, leaky alternative mRNA splicing, and CFTR protein at the cell membrane. Hum Mutat 14(2):133-44.

Beever CL, Stephenson MD, Penaherrera MS, Jiang RH, Kalousek DK, Hayden M, Field L, Brown CJ, Robinson WP. 2003. Skewed X-chromosome inactivation is associated with trisomy in women ascertained on the basis of recurrent spontaneous abortion or chromosomally abnormal pregnancies. Am J Hum Genet 72(2):399-407.

Bottillo I, Torrente I, Lanari V, Pinna V, Giustini S, Divona L, De Luca A, Dallapiccola B. 2010. Germline mosaicism in neurofibromatosis type 1 due to a paternally derived multi-exon deletion. Am J Med Genet A 152A(6):1467-73.

Crowe FW, Schull WJ, Neel JV. 1956. A clinical, pathological, and genetic study of multiple neurofibromatosis. Springfield (Il): Charles C. Thomas.

Friedman JM GD, Maccollin M, Riccardi VM. 1999. Neurofibromatosis:phenotype, natural history, and pathogenesis,3rd edn. Johns Hopkins University Press, Baltimore.

Gurvich OL, Tuohy TM, Howard MT, Finkel RS, Medne L, Anderson CB, Weiss RB, Wilton SD, Flanigan KM. 2008. DMD pseudoexon mutations: splicing efficiency, phenotype, and potential therapy. Ann Neurol 63(1):81-9.

Ingordo V, D'Andria G, Mendicini S, Grecucci M, Baglivo A. 1995. Segmental neurofibromatosis: is it uncommon or underdiagnosed? Arch Dermatol 131(8):959-60.

Kaminsky ZA, Assadzadeh A, Flanagan J, Petronis A. 2005. Single nucleotide extension technology for quantitative site-specific evaluation of metC/C in GC-rich regions. Nucleic Acids Res 33(10):e95.

Kayes LM, Burke W, Riccardi VM, Bennett R, Ehrlich P, Rubenstein A, Stephens K. 1994. Deletions spanning the neurofibromatosis 1 gene: identification and phenotype of five patients. Am J Hum Genet 54(3):424-36.

Kehrer-Sawatzki H, Cooper DN. 2008. Mosaicism in sporadic neurofibromatosis type 1: variations on a theme common to other hereditary cancer syndromes? J Med Genet 45(10):622-31.

Kimani JW, Shi M, Daack-Hirsch S, Christensen K, Moretti-Ferreira D, Marazita ML, Field LL, Canady JW, Murray JC. 2007. X-chromosome inactivation patterns in monozygotic twins and sib pairs discordant for nonsyndromic cleft lip and/or palate. Am J Med Genet A 143A(24):3267-72.

Lazaro C, Ravella A, Gaona A, Volpini V, Estivill X. 1994. Neurofibromatosis type 1 due to germ-line mosaicism in a clinically normal father. N Engl J Med 331(21):1403-7.

Lopez Correa C, Brems H, Lazaro C, Estivill X, Clementi M, Mason S, Rutkowski JL, Marynen P, Legius E. 1999. Molecular studies in 20 submicroscopic neurofibromatosis type 1 gene deletions. Hum Mutat 14(5):387-93.

Lyon MF. 1961. Gene action in the X-chromosome of the mouse (Mus musculus L.). Nature 190:372-3.

Lyon MF. 1962. Sex chromatin and gene action in the mammalian X-chromosome. Am J Hum Genet 14:135-48.

Maertens O, De Schepper S, Vandesompele J, Brems H, Heyns I, Janssens S, Speleman F, Legius E, Messiaen L. 2007. Molecular dissection of isolated disease features in mosaic neurofibromatosis type 1. Am J Hum Genet 81(2):243-51.

Maertens O, Legius E, Speleman F, Messiaen L, Vandesompele J. 2006. Real-time quantitative allele discrimination assay using 3' locked nucleic acid primers for detection of low-percentage mosaic mutations. Anal Biochem 359(1):144-6.

Mautner VF, Kluwe L, Friedrich RE, Roehl AC, Bammert S, Hogel J, Spori H, Cooper DN, Kehrer-Sawatzki H. 2010. Clinical characterisation of 29 neurofibromatosis type-1 patients with molecularly ascertained 1.4 Mb type-1 NF1 deletions. J Med Genet 47(9):623-30.

Messiaen LaW, K. 2008. NF1 mutational Spectrum. In: Kaufmann D, editor. Neurofibromatoses. Monographs in Human genetics. p 63-77

Moss C, Green SH. 1994. What is segmental neurofibromatosis? Br J Dermatol 130(1):106-10.

Nissim-Rafinia M, Kerem B. 2005. The splicing machinery is a genetic modifier of disease severity. Trends Genet 21(9):480-3.

Pasmant E, Sabbagh A, Spurlock G, Laurendeau I, Grillo E, Hamel MJ, Martin L, Barbarot S, Leheup B, Rodriguez D, Lacombe D, Dollfus H, Pasquier L, Isidor B, Ferkal S, Soulier J, Sanson M, Dieux-Coeslier A, Bieche I, Parfait B, Vidaud M, Wolkenstein P, Upadhyaya M, Vidaud D. 2010. NF1 microdeletions in neurofibromatosis type 1: from genotype to phenotype. Hum Mutat 31(6):E1506-18.

Pros E, Fernandez-Rodriguez J, Canet B, Benito L, Sanchez A, Benavides A, Ramos FJ, Lopez-Ariztegui MA, Capella G, Blanco I, Serra E, Lazaro C. 2009. Antisense therapeutics for neurofibromatosis type 1 caused by deep intronic mutations. Hum Mutat 30(3):454-62.

Raedt TM, O.; Serra, E. ; Legius, E. 2008. Somatic NF1 Mutations in Tumors and Other Tissues vol 16:143-153

Riccardi VM. 1982. Neurofibromatosis: clinical heterogeneity. Curr Probl Cancer 7(2):1-34.

Riccardi VM. 1992. Neurofibromatosis: Phenotype, Natural History and Pathogenesis. Baltimore: Johns Hopkins University Press.

Ruggieri M, Huson SM. 2001. The clinical and diagnostic implications of mosaicism in the neurofibromatoses. Neurology 56(11):1433-43.

Ruggieri M, Polizzi A. 2000. Segmental neurofibromatosis [letter]. J Neurosurg 93(3):530-2.

Serra E, Ars E, Ravella A, Sanchez A, Puig S, Rosenbaum T, Estivill X, Lazaro C. 2001. Somatic NF1 mutational spectrum in benign neurofibromas: mRNA splice defects are common among point mutations. Hum Genet 108(5):416-29.

Sharp A, Robinson D, Jacobs P. 2000. Age- and tissue-specific variation of X chromosome inactivation ratios in normal women. Hum Genet 107(4):343-9.

Uhlmann K, Brinckmann A, Toliat MR, Ritter H, Nurnberg P. 2002. Evaluation of a potential epigenetic biomarker by quantitative methyl-single nucleotide polymorphism analysis. Electrophoresis 23(24):4072-9.

Upadhyaya M, Huson SM, Davies M, Thomas N, Chuzhanova N, Giovannini S, Evans DG, Howard E, Kerr B, Griffiths S, Consoli C, Side L, Adams D, Pierpont M, Hachen R, Barnicoat A, Li H, Wallace P, Van Biervliet JP, Stevenson D, Viskochil D, Baralle D, Haan E, Riccardi V, Turnpenny P, Lazaro C, Messiaen L. 2007. An absence of cutaneous neurofibromas associated with a 3-bp inframe deletion in exon 17 of the NF1 gene (c.2970-2972 delAAT): evidence of a clinically significant NF1 genotype-phenotype correlation. Am J Hum Genet 80(1):140-51.

Wang X, Wang M, MacLennan GT, Abdul-Karim FW, Eble JN, Jones TD, Olobatuyi F, Eisenberg R, Cummings OW, Zhang S, Lopez-Beltran A, Montironi R, Zheng S, Lin H, Davidson DD, Cheng L. 2009. Evidence for common clonal origin of multifocal lung cancers. J Natl Cancer Inst 101(8):560-70.

Wolkenstein P, Mahmoudi A, Zeller J, Revuz J. 1995. More on the frequency of segmental neurofibromatosis [letter; comment]. Arch Dermatol 131(12):1465.

Zlotogora J. 1993. Mutations in von Recklinghausen neurofibromatosis: an hypothesis. Am J Med Genet 46(2):182-4.

Figure Legends

Figure 1

Patient and mutation description, SNaPshot results and XCI assay. **A:** Pedigree of the patient (Left panel). Detail of neurofibromas from the back where the small size of them can be appreciated (Right panel). **B:** Schematic representation of the *NF1* deep intronic mutation (c.3198-314G>A) and the observed aberrant splicing. Constitutive and cryptic exons are represented by dark and light grey boxes, respectively. Mutated nucleotide is shown in capital letter and indicated by an arrow. Intron sequences are in lower case; boxes in introns mark cryptic splice sites. **C**: Summary of the SNaPShot results for mutation c.3198-314G>A (light grey bars) and the SNP rs2075786 (control SNP) (dark grey bars) in a battery of different samples from our patient. Allele proportion is indicated on the Y-axis, experiments were performed in triplicate. Data are represented by a bar consisting of the mean±SD. **D**: Summary of the X-chromosome inactivation assay from different tissues of the studied patient and controls. Results were averaged from at least two replicates of the experiment.

Figure 2

Quantification of transcripts, minigene assay and AMO treatment. **A:** RT-PCR analysis of total RNA was performed using specific primers to analyze the three types of transcripts produced (wild-type and two aberrant transcripts). The Y-axis of each graph shows the proportion of aberrant transcripts versus the total. Results are represented by a bar consisting of the mean for at least three independent experiments. Upper panel**:** Results from fresh tissues. Lower panel**:** Results from cultured lymphocytes and fibroblasts. P: Puromycin. **B:** Results of the RT-PCR analysis of the two constructed minigenes. MUT: corresponds to the minigene carrying mutation c.3198-314A; WT: correspond to the minigene with the normal sequence (c.3198-314G); C-: negative control. **C:** Correction of *NF1* aberrant splicing and restoration of the neurofibromin function by AMOs. Upper panel: RT-PCR analysis shows the proportion of aberrant transcripts versus the total in the Y-axis. Results are represented by a bar consisting of

the mean±SD for at least three independent experiments. C1: Control, untreated cells from the patient; A: AMO blocking acceptor splice site , D1: AMO blocking Donor 1 splice site , D2: AMO blocking Donor 2 splice site , A+D1+D2: Combined AMOs blocking the three splice sites, C2: unspecific AMO blocking a donor splice site created by a different mutation located in intron 3 of the *NF1* gene. Bottom panel: Morpholino treatment shows reduction of Ras-GTP levels in fibroblast cell cultures from the patient.

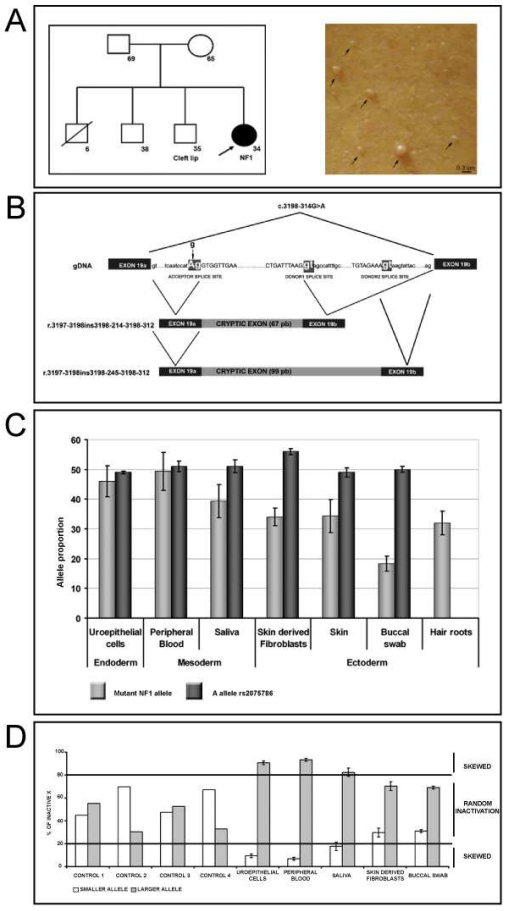

100x100mm (300 x 300 DPI)

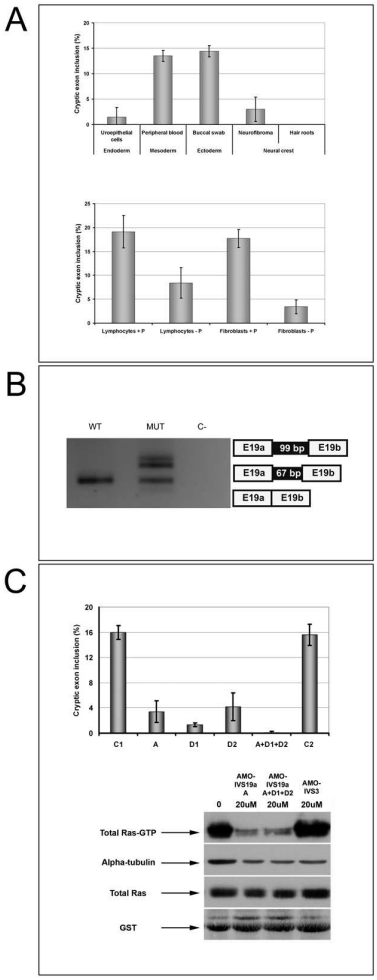

84x169mm (300 x 300 DPI)

MATERIALS AND METHODS

Sample collection and DNA extraction

Different samples belonging to tissues derived from the three embryonic layers were acquired from the studied patient. Skin biopsy, buccal epithelium and hair roots were acquired for ectoderm representation, peripheral blood and saliva for mesoderm, and urine samples to obtain uroepithelial cells detached from the bladder were collected for endoderm representation. Genomic DNA was extracted by using the Gentra purogene kit (Qiagen) except for the saliva, which was extracted by using the Oragene DNA (Genotek), following the manufacturer's instructions.

Mutation has been named according to the Human Genome Variation Society guidelines (http//:www.hgvs.org) and sequence variations checked by Mutalyzer – sequence variant nomenclature check V1.0.1. program (http//:www.LOVD.nl/mutalyzer/). The first nucleotide of the first methionine codon is denoted position +1 according to the NF1 mRNA sequence RefSeq NM_000267.2. Exons are not named consecutively but according to the accepted nomenclature used by researchers in the NF1 field.

SNaPshot Analysis

SNaPshot is a primer extension method based on the addition of a single dye-labelled dideoxy nucleotide to primers localized adjacent to the nucleotide under examination [Kaminsky, et al., 2005; Uhlmann, et al., 2002]. Primer sequences flanking the *NF1* mutation present in intron 19a and flanking an intronic SNP on chromosome 5 (*rs2075786*) in the *hTERT* gene (human telomerase retrotranscriptase) were used, all primers are available upon request. Single nucleotide primer extension reaction was carried out with the SNaPshot Multiplex kit (Applied Biosystems) according to manufacturer's instructions. Products were run in an ABI Prism 3130 DNA Sequencer and analyzed by GeneMapper v4.0 (Applied Biosystems). The degree of mosaicism was calculated using peak heights: Proportion of mutant allele A=A/(A+kG), where A was the peak height of the mutant allele, G the peak height of the wild type allele, and k

was a constant given by the ratio of A/G in heterozygous control samples. Three independent replicates of all experiments were obtained and in every experiment controls were included.

Heterozygous control samples

Artificial heterozygous control samples were created in order to simulate a patient with the same mutation studied in a non-mosaic state to obtain the constant necessary to estimate the proportion of the mutant allele in all the DNA samples studied. PCR products were amplified from the heterozygous patient, with the primers amplifying the studied mutation, and cloned into PCR 2.1 TOPO by the TOPO TA CLONING kit (Invitrogen). Purified constructs were used as homozygous wild type and mutant plasmids. The genotype of the two constructed plasmids was confirmed by DNA sequencing.

X-chromosome inactivation assay

We performed the human androgen-receptor X-inactivation assay as previously described [Allen, et al., 1992]. Briefly, 100 ng of each female genomic DNA sample was digested either with the methylation-sensitive restriction enzyme *Hpa*II (New England Biolabs, Inc., Ipswich, MA) or incubated with 1× enzyme buffer only. Digestion was held for 16h at 37ºC and was then terminated by incubating the reaction at 65ºC for 20 min. From those reactions, one nanogram of each was then amplified by PCR with primers flanking the polymorphic androgen receptor CAG repeat. All reactions were performed at least in duplicate and primers are available upon request. PCR products were analyzed with ABI 3100 Genetics Analyzer (Applied Biosystems). The proportion of inactivation of the lower molecular weight allele (allele 1) was calculated using the following formula, which normalizes occasional biases in allele amplification: Proportion $_{(\text{allele } 1)}$ = ((d1/u1)/(d1/u1+d2/u2)) x 100, where d1 and d2 represent the two peak heights from the digested samples and u1 and u2 are the corresponding peaks from the undigested samples. Results were averaged from two replicates of the experiment. By convention, mildly skewed XCI was defined by an allele ratio >80-20%

and extremely skewed XCI was defined by an allele ratio >90-10% [Beever, et al., 2003; Kimani, et al., 2007].

Cell lines and cultures

For fibroblast isolation, skin was cut into small pieces and digested with 160 U/ml collagenase type 1 (Sigma, St. Louis, MO) and 0.8 U/ml dispase grade 1 (Roche Diagnostics, Penzberg, Germany [Serra, et al., 2001]. Fibroblasts were grown with Dulbecco's modified Eagle's medium (DMEM; Gibco, Invitrogen, Paisley, UK), 10% fetal bovine serum (FBS; Gibco, Invitrogen), and penicillin/streptomycin (Gibco, Invitrogen) at 37ºC and 5% CO_2.

RNA preparation, RT-PCR, and quantification of *NF1* expression

Total RNA was extracted by using the RNeasy Mini Kit (Qiagen, Heidelberg, Germany) following the manufacturer's instructions after the addition of Puromycin (0.25mg/ml for 4h) to prevent the nonsense mRNA decay mechanism (NMD). Reverse-transcription reactions were performed with random hexamers and SuperScript II Reverse Transcriptase (Invitrogen). PCR reactions were performed under the following conditions: 30 cycles of 94ºC for 30 sec, 60ºC for 30 sec, and 72ºC for 1 min after an initial denaturation of 3 min, and followed by a final extension of 8 min. Primer sequences used to amplify both wild-type transcripts and the different transcripts with cryptic exon inclusion are available upon request. PCR products were analyzed with the Agilent 2100 bioanalyzer with DNA 1000 LabChip kit series II (Agilent Technologies, Waldbronn, Germany). Percentages of cryptic exon inclusion were obtained by taking the sum of concentration values (nmol/l) of the different fragments (wild-type and aberrantly spliced) as 100%.

Minigene constructs, transfection, and splicing analysis

The *NF1* minigene containing genomic sequence from exons 19a to 19b was created by cloning an amplified fragment of genomic *NF1* into pcDNA3.1-TOPO (Invitrogen), primers are available upon request. 293-HEK Cells were transfected with 1 µg of plasmid by the use of Lipofectamine (Invitrogen). After 24h, cells were harvested and

RNA extracted using RNeasy kit (Qiagen). Semiquantitative amplification of spliced transcripts was carried out.

Morpholino oligomer design and treatment

The 25-mer AMOs were designed, synthesized, and purified by Gene Tools (Philomath, OR) and targeted the newly created aberrant acceptor splice site (AMO-IVS19a A) and the two different silent donor splice sites (AMO-IVS19a D1 and D2). Endo-Porter (GeneTools) was used to deliver AMOs into cells. AMO sequences are available upon request. In this work we also used an unspecific AMO to evaluate the specificity of our designed AMOs. This unspecific AMO is designed to block a donor splice site generated by a mutation in intron 3 of the *NF1* gene (c.288+2025T>G) [Pros, et al., 2009]. For fibroblast cell line treatment with AMOs, cells were seeded at $3x10^5$ cells/well, in a 6-well plate. The next day, culture medium was replaced by fresh 10% FBS/DMEM medium containing 20 µM of AMOs. Immediately afterwards, Endo-Porter was added and mixed well (6 mM).

Ras-GTP assay and western blot of total Ras

The Ras activation assay kit (Upstate Biotech, Lake Placid, NY) was used according to the manufacturer's protocol. The assay uses affinity precipitation to isolate Ras-GTP from cell lysate. Fibroblast cell lysate (300 µg) was incubated with an agarose-bound Raf-1 RBD fusion protein. Agarose beads were collected by pulsing in a microcentrifuge (5 sec at 14,000 rpm, 3g), washed with lysis buffer, and resuspended in Laemmli sample buffer. Cell lysates containing 5 µg of protein were prepared for Western blot analysis of total Ras. Samples from the Ras-GTP assay and total Ras analysis were then boiled for 5 min and loaded onto 12% SDS-PAGE polyacrylamide gels. Samples were electrophoresed and transferred (400 mA) to a nitrocellulose membrane (Hybond-C extra, GE-Healthcare). The membrane was blocked with 5% non-fat dry milk and incubated overnight at 4ºC with primary antibody, anti-Ras clone RAS10 (1/300; Upstate Biotechnology, Lake Placid, NY) (1 µg/ml). This was followed by incubation with HRP-conjugated secondary antibody at room temperature for 1h.

The blot was developed using the West Pico SuperSignal substrate (Pierce) for the total Ras analysis and Tubulin and West Femto SuperSignal for the Ras-GTP assay.

Supplementary Figure Legends

Supp. Figure S1

SNaPshot results from two different homozygous clones mixed to obtain different allele proportions. On the right of every SNaPshot graph the Sanger sequence is observed. The asterisk denotes the position of the mutation under examination. Numbers indicate the ratio between the wild type and mutant allele.

Supp. Figure S2

Regression analysis of SNaPshot analysis of c.3198-314G>A mutation after mixing two homozygous control cDNAs in different proportions. Allele proportions were calculated from the peak heights: Proportion of A allele= A/(A+kG) where the correction factor k is determined from the mix simulating an allele proportion of 0.5 (5:5). The measured allele frequencies were plotted against the expected allele frequencies. A near linear relationship over the whole data is confirmed (R^2=0.998).

Supp. Figure S3

Results from SNaPShot analysis of c.3198-314G>A mutation in different samples. The asterisk denotes the position of the mutation under examination.

Supp. Figure S4

Results from SNaPShot analysis of rs 2075786 in different samples. The asterisk denotes the position of the mutation under examination.

Supp. Figure S5

Results from X-Chromosome Inactivation (XCI) Assay. **A:** Analysis of the XCI pattern in blood from four different controls. **B:** Analysis of the XCI pattern in different samples of the studied patient. U: undigested, D: digested.

Supp. Figure S6

Schematic representation of the wild type and mutant minigenes and their corresponding splicing. Solid line corresponds to the expected splicing, and dashed line corresponds to the wild-type splicing from the mutant allele that we are assessing

with this minigene analysis. E19a: Exon 19a, E19b: Exon 19b, I19a: Intron 19a, D1: Donor 1 cryptic splice site, D2: Donor 2 cryptic splice site.

Supp. Figure S7

Schematic representation of the three cryptic splice sites located deep inside intron 19a that allow the insertion of two aberrant transcripts: CEI1 and CEI2. And a graph showing the proportion of the two cryptic exon transcrits (CEI1 and CEI2); underneath the Agilent electrophoresis gel is shown.

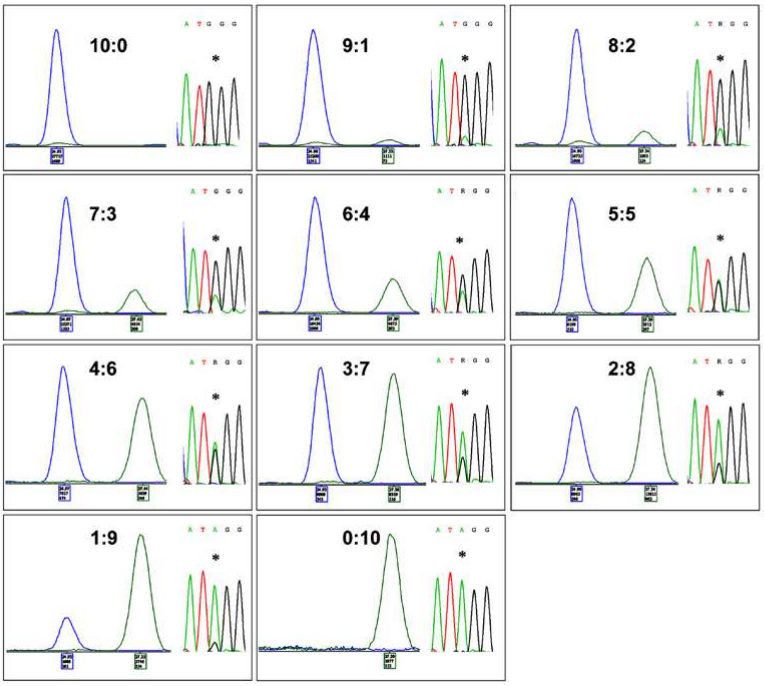

84x70mm (300 x 300 DPI)

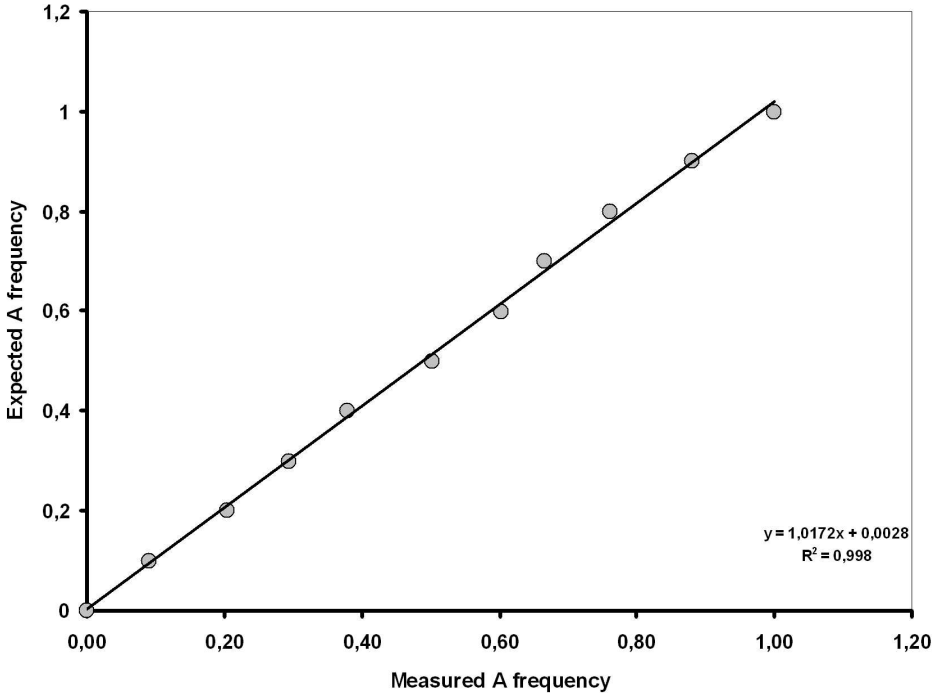

90x70mm (500 x 500 DPI)

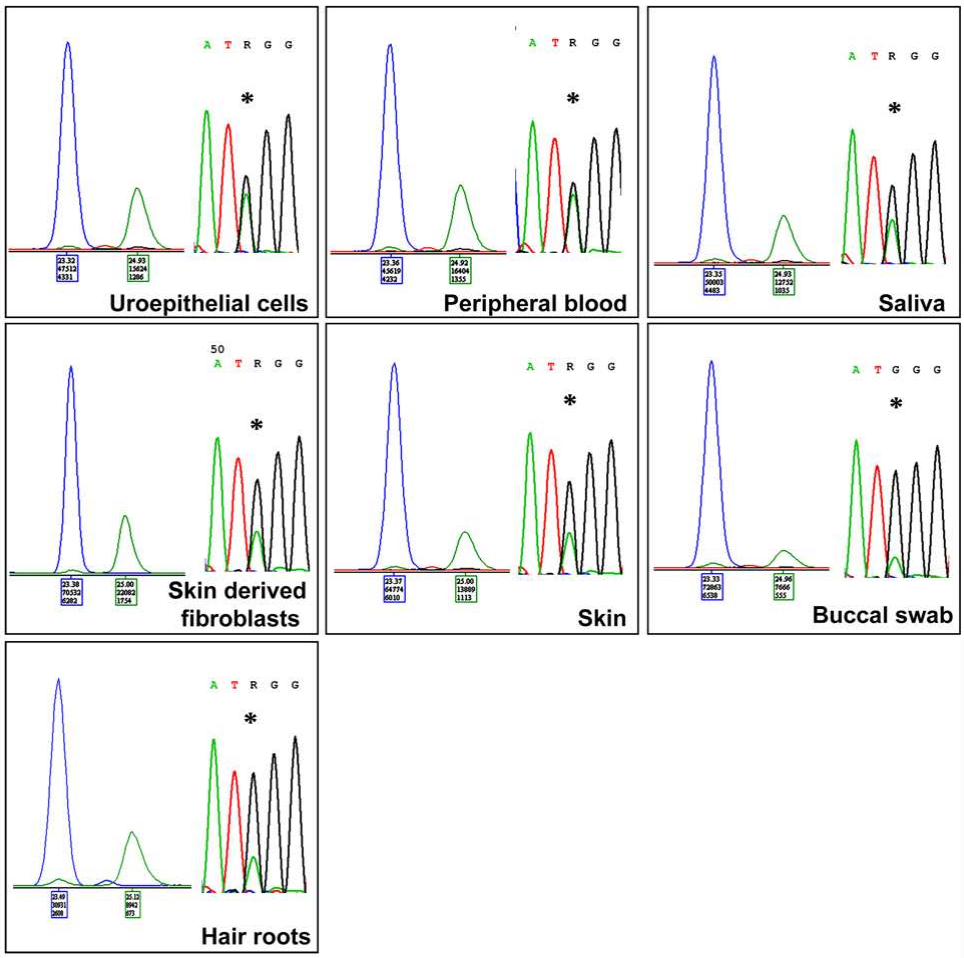

84x82mm (300 x 300 DPI)

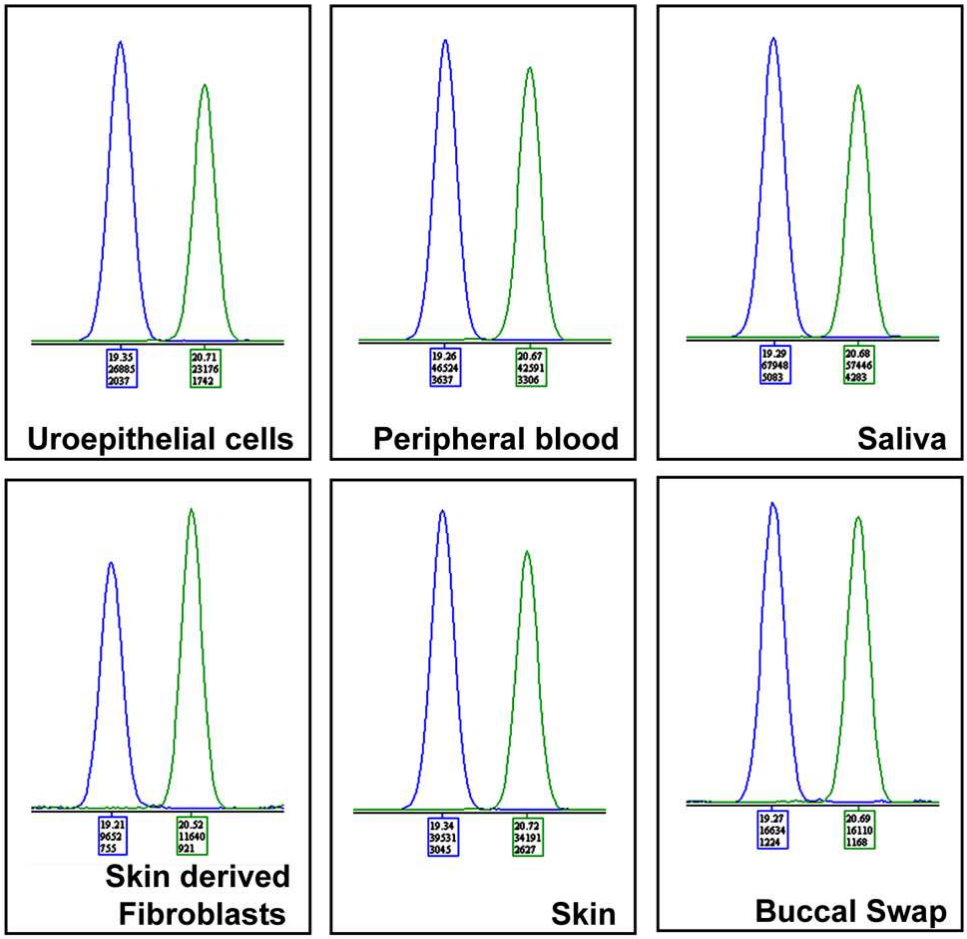

84x81mm (300 x 300 DPI)

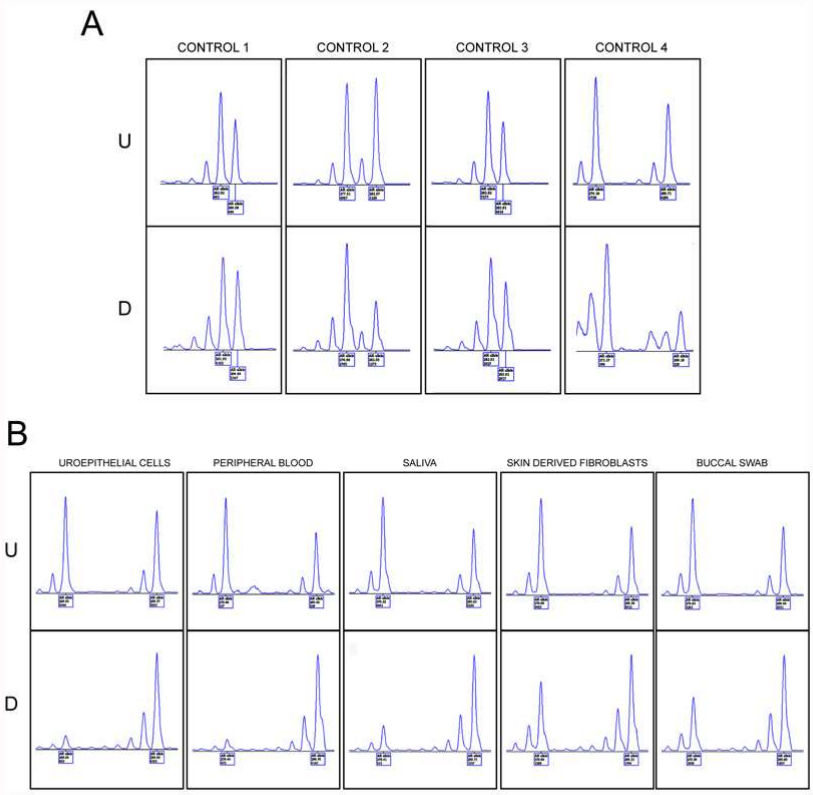

84x84mm (300 x 300 DPI)

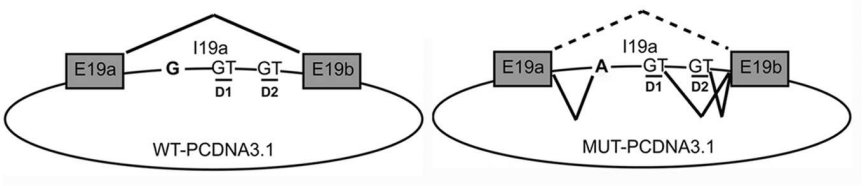

133x62mm (300 x 300 DPI)

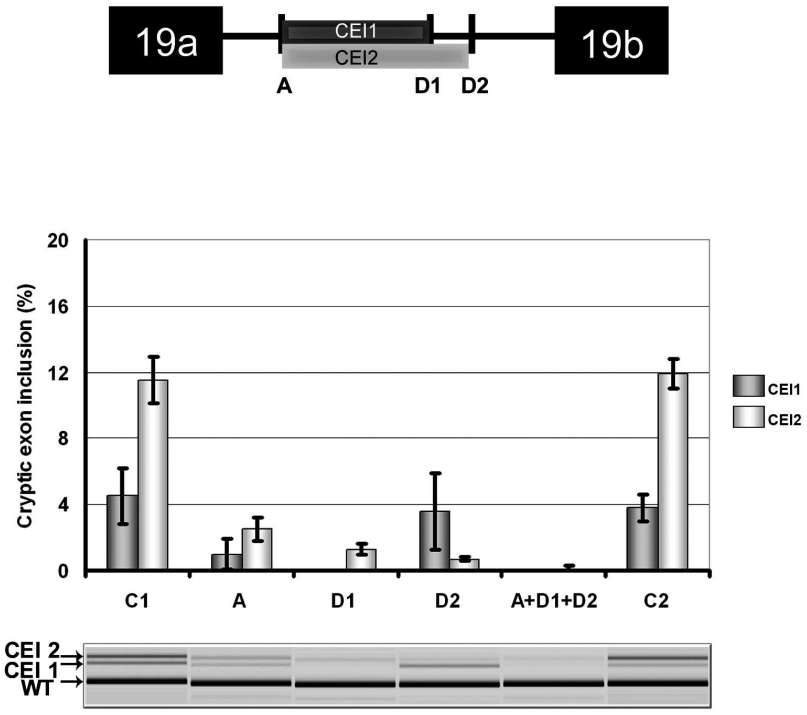

161x144mm (300 x 300 DPI)

Supp. Table S1: Description of the *NF1* deep intronic mutation at genomic, mRNA and protein levels.

DNA Mutation	Intron	mRNA effect	Putative protein
c.3198-314G<A	19a	r.3197-3198ins3198-214-3198-312 r.3197-3198ins3198-245-3198-312	p.Asp1067Trp fsX7

Supp. Table S2: Summary of the predicted scores for the cryptic sites used by the identified mutation.

	3' splice-site (acceptor) sequences and scores					5' splice-site (donor) sequences and scores				
DNA Mutation	Sequence	S&S	NN	ME	MM	Sequence	S&S	NN	ME	MM
c.3198-314G>A	(**A**) CAAATATTTTCAATCCAT**A**G GTG **mut**	84,57	0,95	9,05	8,41	(**D1**) AAG **GT**AGCC	71,29	0,8	7,58	5,31
	CAAATATTTTCAATCCATGG GTG **wt**	68,02	0	-22,81	-16,3	(**D2**) AAA **GT**AAGT	87,84	0,99	9,72	8,51

Nucleotide introduced by mutation is in bold. Splice-site strength scores are obtained using the Shapiro and Senapathy (S&S) consensus splice-site weight matrix, neural network (NN) prediction, first-order Markov models (MM), and a maximum entropy (ME) model. A higher score indicates a greater probability of the resulting sequence being used as a splice site. **A**: Acceptor splice site, **D1**: Donor 1 cryptic splice site, **D2**: Donor 2 cryptic splice site.